Energy & Environmental Science

RSC Publishing

COMMUNICATION

Texturation boosts the thermoelectric performance of BiCuSeO oxyselenides†

Cite this: *Energy Environ. Sci.*, 2013, **6**, 2916

Received 31st May 2013
Accepted 23rd July 2013

DOI: 10.1039/c3ee41859f

www.rsc.org/ees

Jiehe Sui,[a] Jing Li,[a] Jiaqing He,*[b] Yan-Ling Pei,[c] David Berardan,[d] Haijun Wu,[e] Nita Dragoe,[d] Wei Cai[a] and Li-Dong Zhao‡*[d]

We present a high $ZT \sim 1.4$ in textured $Bi_{0.875}Ba_{0.125}CuSeO$ obtained by a hot-forging process. The carrier mobility along the direction perpendicular to the pressing direction was significantly increased, resulting in increase in the electrical conductivity and maximization of the power factor at 923 K from 6.3 $\mu W\ cm^{-1}\ K^{-2}$ for the sample before hot-forging to 8.1 $\mu W\ cm^{-1}\ K^{-2}$ after the hot-forging process. Therefore, the maximum ZT was significantly increased from ~1.1 to 1.4 through texturing for $Bi_{0.875}Ba_{0.125}CuSeO$, which is the highest ZT ever reported among oxygen containing materials.

Thermoelectric materials, capable of converting waste heat into electrical power, are relevant to sustainable energy generation and are currently receiving a significant scientific attention. The efficiency of thermoelectric devices is determined by the dimensionless figure of merit (ZT), defined as $ZT = (S^2\sigma/\kappa)T$, where S, σ, κ, and T are the Seebeck coefficient, the electrical conductivity, the thermal conductivity, and the absolute temperature, respectively. To date, most of the discovered bulk materials with high ZT values exhibit thermal and chemical instability in air at elevated temperature,[1–8] and contain toxic, scarce or expensive elements. Nevertheless, oxides could be potential candidates in the thermoelectric applications on the basis of their advantages over heavy metallic alloys in chemical and thermal robustness. Recently, we have reported a promising thermoelectric system, quaternary oxyselenides BiCuSeO,[9] whose high ZT values largely outperform those of other oxides due to its intrinsically low thermal conductivity.[11] It indicates that the best way to enhance thermoelectric performance ZT is to increase electrical transport properties. Indeed, the ZT has been improved by increasing carrier concentration through optimizing dopants.[10] However, the low carrier mobility of 20 $cm^{-2}\ V^{-1}\ s^{-1}$ for pristine BiCuSeO limits the improvement of electrical transport properties. Moreover, the carrier mobility was deteriorated by carrier–carrier scattering after heavily doping, resulting in a moderate power factor. For example, our extensive studies of the group IIA elements (Mg, Ca, Sr and Ba)

Broader context

Thermoelectric power generation technology is hopefully expected to relax global energy problems by harvesting and converting waste heat into electricity. Thermoelectric oxides, composed of nontoxic, naturally abundant, light, and cheap elements, are expected to play a vital role in extensive applications for waste heat recovery in an air atmosphere. The thermoelectric conversion efficiency is decided by a "goodness factor" of ZT. We present a high $ZT \sim 1.4$ in textured $Bi_{0.875}Ba_{0.125}CuSeO$ prepared by a hot-forging process. The textured microstructure, with preferred grain orientation, was observed using X-ray diffraction and scanning electron microscopy equipped with an electron back-scatter diffraction detector. After the hot-forging process, the carrier mobility along the direction perpendicular to the pressing direction was significantly increased, resulting in an increased electrical conductivity and a maximized power factor at 923 K from 6.3 $\mu W\ cm^{-1}\ K^{-2}$ for the sample before hot-forging to 8.1 $\mu W\ cm^{-1}\ K^{-2}$ after the hot-forging process. Although the corresponding total thermal conductivity was increased after hot-forging, this increment was more than compensated by the improved electrical conductivity. Therefore, the maximum ZT was significantly increased from 1.1 for $Bi_{0.875}Ba_{0.125}CuSeO$ to 1.4 for the sample after three steps of the hot-forging process, which is the highest ZT ever reported among oxygen containing materials.

[a]*National Key Laboratory Precision Hot Processing of Metals, School of Materials Science and Engineering, Harbin Institute of Technology, Harbin 150001, China*

[b]*Department of Physics, South University of Science and Technology of China, Shenzhen 518055, China. E-mail: he.jq@sustc.edu.cn*

[c]*School of Materials Science and Engineering, Beihang University, Beijing 100191, China*

[d]*LEMHE, ICMMO (CNRS UMR 8182), Univ. Paris Sud, Orsay F91405, France. E-mail: lidong-zhao@northwestern.edu*

[e]*Frontier Institute of Science and Technology (FIST), Xi'an Jiaotong University, Xi'an 710054, China*

† Electronic supplementary information (ESI) available: Experimental details, and the typical textured samples used in this study (Fig. S1); cross-section orientation maps of $Bi_{0.875}Ba_{0.125}CuSeO$ samples before and after hot-forging (Fig. S2 and S3); temperature dependence on heat capacity, thermal diffusivity, Lorenz numbers, and electronic thermal conductivity (Fig. S4) for textured $Bi_{0.875}Ba_{0.125}CuSeO$ samples. See DOI: 10.1039/c3ee41859f

‡ L.-D. Zhao is presently in Department of Chemistry, Northwestern University, Evanston, Illinois 60208, USA.

as dopants[9,10] indicate that heavy hole doping is very effective for *ZT* enhancement, with a carrier concentration as high as $\sim 1 \times 10^{21}$ cm^{-3}, but it is at the cost of a reduced carrier mobility down to 1–2 cm^{-2} V^{-1} s^{-1}.

Oxyselenides crystallize in a layered crystal structure that is constituted by conductive $(Cu_2Se_2)^{2-}$ layers alternately stacked with insulating $(Bi_2O_2)^{2+}$ layers along the *c* axis. Therefore, the electrical and thermal transport in the BiCuSeO system should be anisotropic,[9,10] and a higher carrier mobility in the *a*, *b* plane (in-plane) than that in the *c* direction (cross-plane) can be expected, which could be similar to the anisotropy observed in Bi_2Te_3 and $CaCoO_3$ compounds with a layered structure.[12] Thus, a promising way to further enhance *ZT* would be to take advantage of this anisotropy, by applying a hot-forging process, to produce the *a*, *b* plane of the grains oriented along a certain direction through sample deformation under external applied pressure in order to improve the carrier mobility. Since the heavily hole doped $Bi_{0.875}Ba_{0.125}CuSeO$ sample exhibits the highest thermoelectric performance among the BiCuSeO system with a *ZT* of 1.1 at 923 K, in this study, it is expected that a higher *ZT* for $Bi_{0.875}Ba_{0.125}CuSeO$ could be obtained by additionally improving the carrier mobility. Finally, a twofold increased carrier mobility has been obtained by the sample texturation through a three step hot-forging process, resulting in a record *ZT* of ~1.4 at 923 K for $Bi_{0.875}Ba_{0.125}CuSeO$, which is the highest value ever reported for oxygen containing materials,[11] pointing to a robust candidate for further medium temperature thermoelectric applications.

Samples were synthesized *via* a two-step solid state reaction route, and the obtained bulk materials were ground into powders followed by several hot forging steps to get textured microstructures. The experimental details including sample synthesis, hot-forging process, thermoelectric property measurements, X-ray diffraction (XRD) phase characterization, and electron backscattering diffraction (EBSD) characterizations are given in the ESI.† Fig. 1 shows the XRD patterns of the sample's section perpendicular to the pressing direction for textured $Bi_{0.875}Ba_{0.125}CuSeO$ before and after hot-forging, and the inset shows the crystal structure of BiCuSeO. The scheme of the hot-forging process and the typical samples used in this study can be found in Fig. S1.† In order to express expediently in the text, the as-synthesized, one-step, two-step and three-step hot-forged samples with textured microstructures were shortly named 0T, 1T, 2T and 3T, respectively. Correspondingly, the textured samples cut perpendicular and parallel to the pressing direction were named *x*T-⊥ (radial direction in a cylinder sample, as shown in Fig. S1†) and *x*T-∥ (axial direction in a cylinder sample, *x* is the number of hot-forging steps, $x = 0, 1, 2, 3$), respectively. For example, 2T-⊥ is a sample prepared by 2 hot-forging steps and cut perpendicular to the pressing direction. All characteristic peaks can be indexed in the ZrSiCuAs structure type, indicating the formation of single phase $Bi_{0.875}Ba_{0.125}CuSeO$ compounds. The grain orientation experiences a significant difference after the hot-forging process. Indeed, the hot-forged samples (1T-⊥, 2T-⊥, 3T-⊥) show much stronger diffraction intensities at (00*l*) Bragg directions such as (003), (004), (005), (006), (007), and (008) than the sample before hot-forging (0T). Typically, the main diffraction peak changes from (102) for the sample before hot-forging (0T) to (003) for the sample after two hot-forging steps. Moreover, the relative intensities of the (00*l*) peaks become much stronger with increasing hot-forging steps (from 0T to 3T), which indicates a better preferential orientation of the grains with the increasing hot-forging steps. The orientation degree can be estimated by the Lotgering method.[12a] The calculated Lotgering factor in this study increases from 0.12 (0T-⊥) to about 0.82 (3T-⊥). This observation confirms that the platelet grains after hot-forging are preferentially oriented with their *a*, *b* plane perpendicular to the pressing direction.

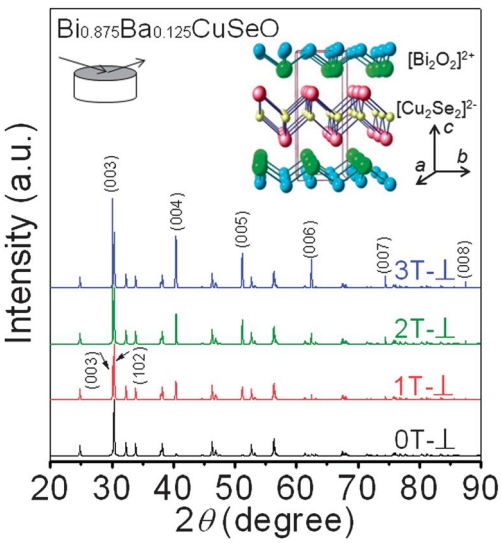

Fig. 1 XRD patterns of textured $Bi_{0.875}Ba_{0.125}CuSeO$; a (*00l*) preferential orientation can be observed after hot-forging. The crystal structure is also plotted showing the $(Cu_2Se_2)^{2-}$ and $(Bi_2O_2)^{2+}$ layers (inset).

Fig. 2 shows the microstructures perpendicular to the pressing direction of $Bi_{0.875}Ba_{0.125}CuSeO$ before and after hot-forging using scanning electron microscopy (SEM) with an EBSD detector. Band contrast-, Euler- and (inverse) pole-images are used to describe the orientation of the textured grains. Fig. 2(a, e, h, and k) show the band contrast images of 0T-⊥, 1T-⊥, 2T-⊥ and 3T-⊥ samples, respectively, where grain size can be measured, as shown in Fig. 2(b, f, i, and l), correspondingly. During hot-forging, the grains experience a slight growth trend with a preferential growth along the *a*, *b* plane (perpendicular to the hot-forging direction). For all-, *X*-, *Y*-, and *Z*-Euler images in Fig. 2, S2 and S3 in the ESI†, grains with red, green and blue colors are oriented along [001], [010] and [110] directions, respectively. The grain orientation in the 0T-⊥ sample (without hot-forging) is nearly isotropic (Fig. 2(c and d)), although a slight preferential orientation along the [001] direction already exists (more grains with near-red color in Fig. 2(c)), because the intrinsic layered crystal structure leads to platelet grains that can be slightly aligned during the uniaxial hot-pressing step. As hot-forging steps increase, the grains' orientation along the [001] direction (red grains in the *Z*-Euler image) is more and more obvious, especially for the 3T-⊥ sample (all near-red grains in the *Z*-Euler image (Fig. 2(m) and S3(d) in the ESI†)), while there are almost away-red grains in the *X*/*Y*-Euler image

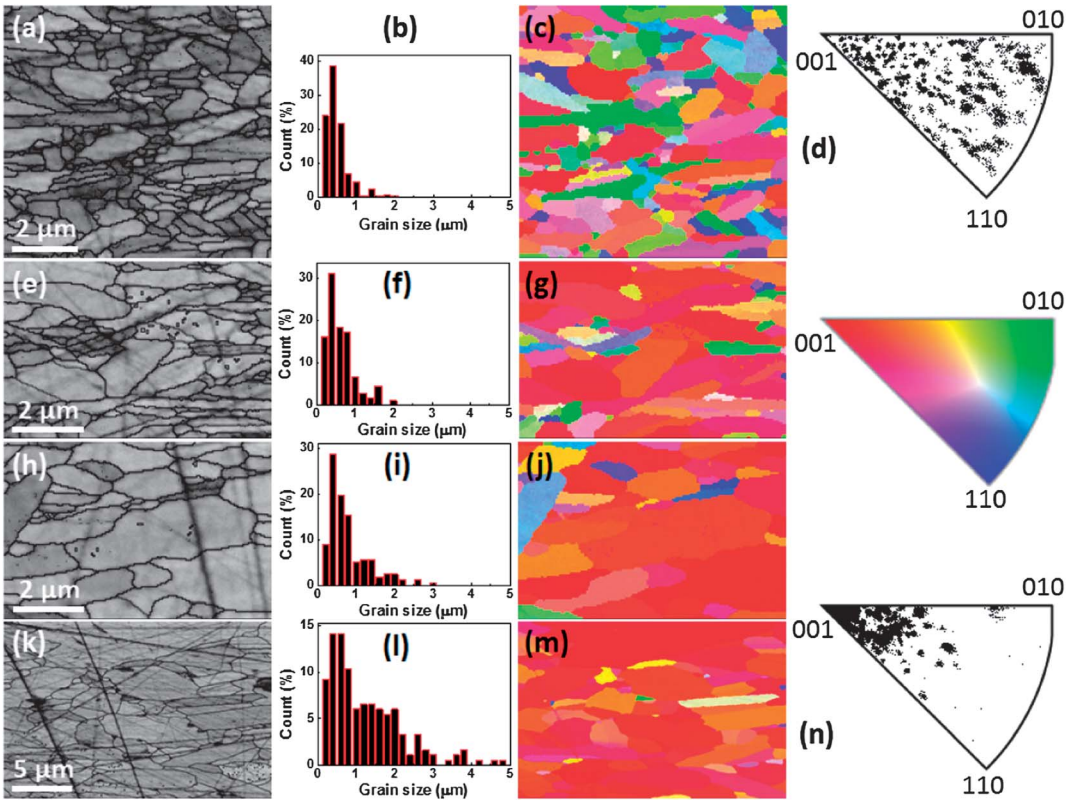

Fig. 2 EBSD microstructures of textured $Bi_{0.875}Ba_{0125}CuSeO$: (a), (e), (h) and (k) band contrast images of 0T-⊥, 1T-⊥, 2T-⊥ and 3T-⊥ samples, respectively. (b), (f), (i) and (l) Grain size distribution histograms of 0T-⊥, 1T-⊥, 2T-⊥ and 3T-⊥ samples, respectively. (c), (g), (j) and (m) *Z*-Euler images of 0T-⊥, 1T-⊥, 2T-⊥ and 3T-⊥ samples, respectively. (d) and (n) Inverse pole figures of 0T-⊥ and 3T-⊥ samples.

(Fig. S2(n and o) and S3(b) in the ESI†). The (inverse) pole figures (Fig. 2(d and n)) clearly reflect the fact that the orientation of grains distributes disorderly before hot-forging (Fig. 2(d) and S2(d) in the ESI†), but mostly along the [001] direction after hot-forging (Fig. 2(n), S2(p) and S3(c and e) in the ESI†).

Fig. 3 shows the temperature dependence of the electrical transport properties for textured $Bi_{0.875}Ba_{0.125}CuSeO$ samples. As shown in Fig. 3(a), the samples without hot-forging (0T-⊥ and 0T-||) exhibit similar electrical conductivity values over the entire temperature range along directions perpendicular and parallel to the pressing direction, indicating almost isotropic electrical transport properties. However, it becomes very different in the case of textured samples after hot-forging. It can be readily seen that the electrical conductivity at room temperature along the perpendicular direction shows a 55% increase from 450 S cm^{-1} to 700 S cm^{-1} after three hot-forging steps (3T-⊥). In contrast, the electrical conductivity for the same sample but along the parallel direction significantly (3T-||) decreases from 400 S cm^{-1} to 200 S cm^{-1} after three hot-forging steps. The Hall effect measurements indicate that all the samples have a similar carrier concentration of $\sim 1 \times 10^{21}$ cm^{-3} since the same composition of $Bi_{0.85}Ba_{0.15}CuSeO$ is maintained. Therefore, the present enhancement of the electrical conductivity is not linked to an increase of the carrier concentration, but it mainly originates from the improvement of the carrier mobility. Indeed, Fig. 3(b) shows that the carrier mobility along the perpendicular direction gradually increases when increasing hot-forging steps, from 2 cm^{-2} V^{-1} s^{-1} for the sample without hot-forging (0T-⊥) to 4 cm^{-2} V^{-1} s^{-1} for the

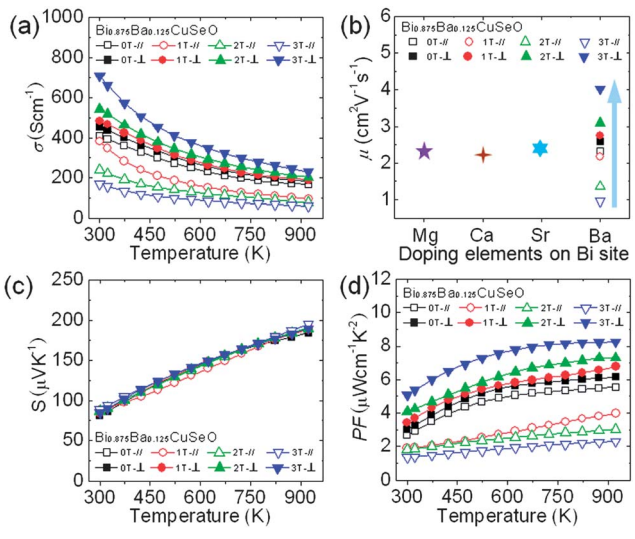

Fig. 3 Electrical transport properties of textured $Bi_{0.875}Ba_{0.125}CuSeO$: (a) electrical conductivity. (b) Room temperature carrier mobility of textured $Bi_{0.875}Ba_{0.125}CuSeO$; the carrier mobilities of Mg,[10e] Ca,[10c] Sr[9] and Ba[10d] doped BiCuSeO samples with similar carrier concentrations are plotted for comparison. (c) Seebeck coefficient. (d) Power factor.

sample after three hot-forging steps (3T-⊥). In contrast, the carrier mobility along the parallel direction shows a decreasing trend after hot-forging. Both XRD and EBSD results evidence a strong texturation in the samples, which indicate that higher mobility in perpendicular direction is clearly linked to the preferential orientation. Interestingly, the hot-forging process has a faint effect on the Seebeck coefficient values, as shown in Fig. 3(c). The positive Seebeck coefficient indicates a p-type electrical transport behavior; Seebeck coefficient values range from +85 μV K^{-1} at 300 K to +187 μV K^{-1} at 923 K for textured $Bi_{0.875}Ba_{0.125}CuSeO$ samples, independent of hot-forging steps and of the measurement direction. Present results indicate that the Seebeck coefficient is isotropic, which is consistent with the constant carrier concentration and with the calculations by Bies and Radtke showing that the Seebeck coefficient is independent of the orientation degree.[13] The combined enhanced electrical conductivity and negligible changes of the positive Seebeck coefficient result in a maximum power factor of ~8.1 μW cm^{-1} K^{-2} at 923 K in the direction perpendicular to the pressing direction after three hot-forging steps (3T-⊥), Fig. 3(d), which corresponds to a 28% increase as compared to the value of 6.3 μW cm^{-1} K^{-2} at 923 K observed for the sample before hot-forging (0T-⊥).

Fig. 4(a) shows the temperature dependence of the total thermal conductivity κ_{tot} for textured $Bi_{0.875}Ba_{0.125}CuSeO$ samples. κ_{tot} is the sum of the electronic (κ_{ele}) and lattice thermal conductivity (κ_{lat}). κ_{ele} can be calculated through the Wiedemann–Franz relation, $\kappa_{ele} = L\sigma T$, where L is the Lorenz number extracted as described previously by fitting of the respective Seebeck values[14,15] (heat capacity, thermal diffusivity, Lorenz number and electronic thermal conductivity κ_{ele} can be found in Fig. S4†). κ_{tot} perpendicular to the pressing direction shows an increasing trend with the increase of hot-forging steps for the textured samples. In contrast, κ_{tot} along the pressing direction shows a decreasing trend with the increase of hot-forging steps. These opposite trends are also observed in the lattice thermal conductivity, Fig. 4(b). Similar to the electrical conductivity, it can be found that the thermal conductivity is higher in the direction perpendicular to the pressing direction (in-plane) than that in the parallel one (cross-plane). Here, it should be noted that both electrical and thermal conductivities are increased perpendicular to the pressing direction by the hot-forging process by producing a textured microstructure, which creates a facile transport path for carriers and phonons.

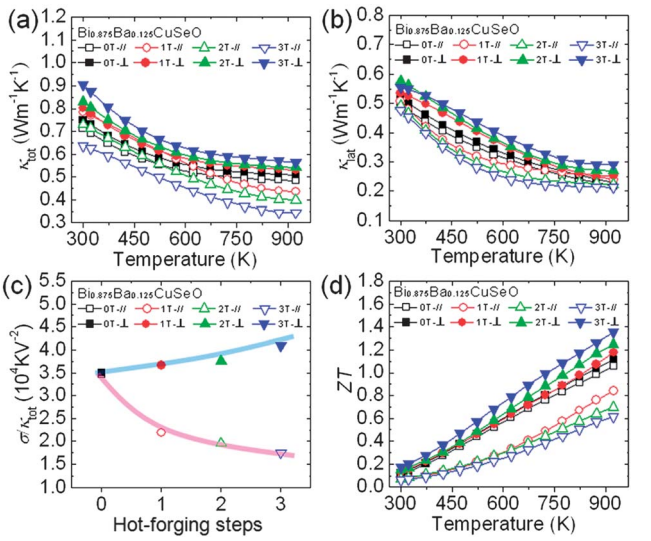

Fig. 4 Thermoelectric properties of textured $Bi_{0.875}Ba_{0.125}CuSeO$: (a) total thermal conductivity. (b) Lattice thermal conductivity. (c) The ratio of electrical to thermal conductivity as a function of the number of hot-forging steps. (d) Figure of merit *ZT*.

The evolution of the transport properties with the hot-forging process could be explained by two different mechanisms. Firstly, BiCuSeO based materials crystallize in a layered crystal structure, with $(Cu_2Se_2)^{2-}$ layers alternately stacked with $(Bi_2O_2)^{2+}$ layers along the *c* axis of the tetragonal unit cell. Regarding the thermal conductivity, this structure should lead to lower values along the *c* axis than within the *a*, *b* plane due to the increased interface concentration along the *c* axis. The same mechanism should be present for the electrical conductivity. However, we have shown previously that the electronic band structure of BiCuSeO exhibits a 3D character,[10f] with a small effective mass difference between the *c* direction and the *a*, *b* plane, which explains the faint variation of the Seebeck coefficient. Secondly, we have seen that the hot-forging process leads both to an anisotropic grain growth with a preferential growth perpendicular to the pressing direction and to an alignment of the platelet grains. Therefore, the grain boundary concentration is decreased perpendicular to the pressing direction (leading to an increase of the electrical conductivity and of the thermal conductivity) and is increased parallel to the pressing direction (leading to an increased phonon and electron scattering rate).

It is well known that the increased thermal conductivity would result in a final *ZT* reduction. Therefore, we need to clarify the ratio of electrical to thermal conductivity as a function of the number of hot-forging steps to highlight the interest in these textured microstructures. As shown in Fig. 4(c), the ratio of the electrical conductivity to the thermal conductivity perpendicular to the pressing direction increases with the number of hot-forging steps. In other words, the increase of the electrical conductivity is larger than that of the thermal conductivity. In contrast, this ratio decreases with increasing number of hot-forging steps in the direction parallel to the pressing direction. This means that a higher *ZT* along the perpendicular direction can be hopefully obtained, because the increased thermal conductivity is more than compensated by the improved electrical conductivity and since Seebeck coefficient does not depend on the texturation. By using the electrical and thermal transport properties, the *ZT* is calculated as shown in Fig. 4(d). As expected, the maximum *ZT* value at 923 K is improved from ~1.1 for $Bi_{0.875}Ba_{0.125}CuSeO$ without texturation to ~1.4 in the perpendicular direction after three hot-forging steps (3T-⊥). This is a record *ZT* value in the BiCuSeO system, which is also higher than any lead free or oxygen containing material reported so far[11] and is close to the values observed in most thermoelectric metallic alloys.[1,2]

In summary, we applied a hot-forging process to produce textured microstructures with the grains preferentially oriented

with the *a*, *b* plane perpendicular to the pressing direction. The texturation results in a two-fold increase in carrier mobility, thus enhancing the electrical conductivity and maximizing the power factor and resulting in a record *ZT* of ~1.4 at 923 K for textured $Bi_{0.875}Ba_{0.125}CuSeO$ after three hot-forging steps. Present results point to a robust candidate for medium temperature thermoelectric applications.

Acknowledgements

This work was supported by National Natural Science Foundation of China (no. 51202008 and 51271069), Major State Basic Research Development Program of China (973 Program, no. 2012CB619400) and Fundamental Research Funds for the Central Universities (no. HIT. BERTIII. 201205). This contribution was also supported in part by the startup of South University of Science and Technology of China funded by Shenzhen government (J. H.) and Program for New Century Excellent Talents in University of Ministry of Education of China (NCET-12-0160) (J. S.).

References

1 (*a*) C. J. Vineis, A. Shakouri, A. Majumdar and M. G. Kanatzidis, *Adv. Mater.*, 2010, **22**, 3970; (*b*) M. G. Kanatzidis, *Chem. Mater.*, 2010, **22**, 648; (*c*) J. G. Snyder and E. S. Toberer, *Nat. Mater.*, 2008, **7**, 105; (*d*) J. P. Heremans, B. Wiendlocha and A. M. Chamoire, *Energy Environ. Sci.*, 2012, **5**, 5510.

2 (*a*) J. F. Li, W. S. Liu, L. D. Zhao and M. Zhou, *NPG Asia Mater.*, 2010, **2**, 152; (*b*) M. Zebarjadi, K. Esfarjani, M. S. Dresselhaus, Z. F. Ren and G. Chen, *Energy Environ. Sci.*, 2012, **5**, 5147; (*c*) J. Q. He, M. G. Kanatzidis and V. P. Dravid, *Mater. Today*, 2013, **16**, 166.

3 B. Poudel, Q. Hao, Y. Ma, Y. Lan, A. Minnich, B. Yu, X. Yan, D. Wang, A. Muto, D. Vashaee, X. Chen, J. Liu, M. S. Dresselhaus, G. Chen and Z. F. Ren, *Science*, 2008, **320**, 634.

4 A. Harnwunggmoung, K. Kurosaki, H. Muta and S. Yamanaka, *Appl. Phys. Lett.*, 2010, **96**, 202107.

5 T. Caillat, J. Fleurial and A. Borshchevsk, *J. Phys. Chem. Solids*, 1997, **58**, 1119.

6 K. F. Hsu, S. Loo, F. Guo, W. Chen, J. S. Dyck, C. Uher, T. Hogan, E. K. Polychroniadis and M. G. Kanatzidis, *Science*, 2004, **303**, 818.

7 K. Biswas, J. Q. He, I. D. Blum, C. I. Wu, T. Hogan, D. N. Seidman, V. P. Dravid and M. G. Kanatzidis, *Nature*, 2012, **489**, 414.

8 B. A. Cook, M. J. Kramer, X. Wei, J. L. Harringa and E. M. J. Levin, *J. Appl. Phys.*, 2007, **101**, 053715.

9 L. D. Zhao, D. Berardan, Y. L. Pei, C. Byl, L. Pinsard-Gaudart and N. Dragoe, *Appl. Phys. Lett.*, 2010, **97**, 092118.

10 (*a*) Y. Liu, L. D. Zhao, Y. C. Liu, J. L. Lan, W. Xu, F. Li, B. P. Zhang, D. Berardan, N. Dragoe, Y. H. Lin, C. W. Nan, J. F. Li and H. M. Zhu, *J. Am. Chem. Soc.*, 2011, **133**, 20112; (*b*) F. Li, J. F. Li, L. D. Zhao, K. Xiang, Y. Liu, B. P. Zhang, Y. H. Lin, C. W. Nan and H. M. Zhu, *Energy Environ. Sci.*, 2012, **5**, 7188; (*c*) Y. L. Pei, J. Q. He, J. F. Li, F. Li, Q. J. Liu, W. Pan, C. Barreteau, D. Berardan, N. Dragoe and L. D. Zhao, *NPG Asia Mater.*, 2013, **5**, e47; (*d*) J. Li, J. H. Sui, Y. L. Pei, C. Barreteau, D. Berardan, N. Dragoe, J. Q. He and L. D. Zhao, *Energy Environ. Sci.*, 2012, **5**, 8543; (*e*) J. Li, J. H. Sui, Y. L. Pei, C. Barreteau, D. Berardan, N. Dragoe, W. Cai and L. D. Zhao, *J. Alloys Compd.*, 2013, **551**, 649; (*f*) C. Barreteau, D. Berardan, E. Amzallag, L. D. Zhao and N. Dragoe, *Chem. Mater.*, 2012, **24**, 3168.

11 (*a*) N. V. Nong, N. Pryds, S. Linderoth and M. Ohtaki, *Adv. Mater.*, 2011, **23**, 2484; (*b*) J. Liu, C. L. Wang, W. B. Su, H. C. Wang, P. Zheng, J. C. Li, J. L. Zhang and L. M. Mei, *Appl. Phys. Lett.*, 2009, **95**, 162110; (*c*) D. Berardan, E. Guilmeau, A. Maignan and B. Raveau, *Solid State Commun.*, 2008, **146**, 97; (*d*) D. Flahaut, T. Mihara, R. Funahashi, N. Nabeshima, K. Lee, H. Ohta and K. Koumoto, *J. Appl. Phys.*, 2006, **100**, 084911; (*e*) M. Ohtaki, K. Araki and K. Yamamoto, *J. Electron. Mater.*, 2009, **38**, 1234; (*f*) M. Shikano and R. Funahashi, *Appl. Phys. Lett.*, 1851, **2003**, 82; (*g*) I. Terasaki, Y. Sasago and K. Uchinokura, *Phys. Rev. B: Condens. Matter Mater. Phys.*, 1997, **56**, 12685; (*h*) K. Fujita, T. Mochida and K. Nakamura, *J. Appl. Phys.*, 2001, **40**, 4644.

12 (*a*) L. D. Zhao, B. P. Zhang, J. F. Li, H. L. Zhang and W. S. Liu, *Solid State Sci.*, 2008, **10**, 651; (*b*) X. Yan, B. Poudel, Y. Ma, W. S. Liu, G. Joshi, H. Wang, Y. C. Lan, D. Z. Wang, G. Chen and Z. F. Ren, *Nano Lett.*, 2010, **10**, 3373; (*c*) Y. H. Lin, J. Lan, Z. J. Shen, Y. H. Liu, C. W. Nan and J. F. Li, *Appl. Phys. Lett.*, 2009, **94**, 072107; (*d*) J. J. Shen, L. P. Hu, T. J. Zhu and X. B. Zhao, *Appl. Phys. Lett.*, 2011, **99**, 124102.

13 W. E. Bies, R. J. Radtke, H. Ehrenreich and E. Runge, *Phys. Rev. B: Condens. Matter Mater. Phys.*, 2002, **65**, 085208.

14 (*a*) L. D. Zhao, S. H. Lo, J. Q. He, H. Li, K. Biswas, J. Androulakis, C.-I. Wu, T. P. Hogan, D. Y. Chung, V. P. Dravid and M. G. Kanatzidis, *J. Am. Chem. Soc.*, 2011, **133**, 20476; (*b*) Y. L. Pei, H. Wu, J. Sui, J. Li, D. Berardan, C. Barreteau, L. Pan, N. Dragoe, W. S. Liu, J. Q. He and L. D. Zhao, *Energy Environ. Sci.*, 2013, **6**, 1750.

15 (*a*) W. S. Liu, Q. Zhang, Y. Lan, S. Chen, X. Yan, Q. Zhang, H. Wang, D. Wang, G. Chen and Z. F. Ren, *Adv. Energy Mater.*, 2011, **1**, 577; (*b*) W. S. Liu, K. C. Lukas, K. McEnaney, S. Lee, Q. Zhang, C. P. Opeil, G. Chen and Z. F. Ren, *Energy Environ. Sci.*, 2013, **6**, 552.

